J. Earth Syst. Sci. (2020)129 211
https://doi.org/10.1007/s12040-020-01478-x

Seasonal variability of tropospheric CO_2 over India based on model simulation, satellite retrieval and *in-situ* observation

M Krishnapriya[1,3], Rabindra K Nayak[1,*], Shaik Allahudeen[1], A Bhuvanachandra[1], V K Dadhwal[2], C S Jha[1], M V R Sheshasai[1], S K Sasmal[1] and K V S R Prasad[3]

[1]*National Remote Sensing Center (NRSC), Indian Space Research Organization (ISRO), Balanagar, Hyderabad 500 037, India.*
[2]*Indian Institute of Space Science and Technology (IIST), Thiruvananthapuram, Kerala, India.*
[3]*Department of Meteorology and Physical Oceanography, Andhra University, Visakhapatnam, India.*
**Corresponding author. e-mail: rabin2005@rediffmail.com rabindrakumar_nayak@nrsc.gov.in*

MS received 11 February 2020; revised 6 June 2020; accepted 9 July 2020

In this study, investigation of the seasonal cycle of the tropospheric CO_2 concentration over India was carried out using the GEOS-Chem atmospheric transport model, Greenhouse gas Observation SATellite (GOSAT) retrievals, and *in-situ* measurements. The model simulation is highly coherent with the satellite and *in-situ* datasets, and it shows a distinct seasonal cycle of the tropospheric CO_2 tendency over India with a negative phase (decreasing concentration) during April–August and a positive phase (increasing concentration) during September–March. The model diagnostics were analyzed to estimate budgets of the surface layer CO_2, up to 650 hPa pressure level, for the two-phases of the seasonal cycle. A mean tendency, equivalent to −0.70 ppmv month^{-1}, observed during April–August, which results from the loss of CO_2 content in the surface layer through horizontal advection (−2.25 ppmv month^{-1}) and vertical diffusion (−0.20 ppmv month^{-1}), that dominates the gain from vertical advection (1.53 ppmv month^{-1}). The negative contribution of horizontal advection in this period comes from the transport of CO_2 depleted air-parcels over the oceanic region to India by the southwest monsoon winds and the positive contributions of vertical advection comes from upwelling of CO_2 enriched air-parcels. The mean tendency, equivalent to 1.01 ppmv month^{-1}, during September–March results from the gain through vertical advection (0.78 ppmv month^{-1}) and horizontal advection (0.37 ppmv month^{-1}) and a small contribution of vertical diffusion (−0.15 ppmv month^{-1}). In this period, positive contribution of horizontal advection is due to the transport of CO_2 enriched air-parcels from the southeast Asian region to India by north-east monsoon winds. At the annual scale, CO_2 content of the surface layer over India has a net gain of 0.75 GtC that comes from 14.31 GtC through vertical advection that exceeds the loss due to horizontal advection (−11.10 GtC) and vertical diffusion processes (−2.46 GtC). This net gain is almost 85% higher than the input of 0.4 GtC through surface fluxes, which composed of 0.61 GtC anthropogenic emission and −0.21 GtC net terrestrial ecosystem exchanges. Additional sensitivity experiment was carried out to elucidate the semi-annual features of the seasonal cycle of CO_2 for north India, in contrast to the annual characteristics of the seasonal cycle for south India in relation to the GOSAT observation.

Keywords. Atmospheric CO_2; seasonal cycle; transport processes; net ecosystem exchanges; GEOS-Chem model; GOSAT; India.

Published online: 15 October 2020

1. Introduction

Carbon dioxide (CO_2) is a major long-lived greenhouse gas in the atmosphere, which plays a significant role in warming the Earth by radiative forcing through entrainment of outgoing long-wave radiations from the surface to the space (Smil 2002). It exhibits variability in a broad range of spatial and temporal scales, with a net increase by about 48% from 280 ppmv in 1750 to 415 ppmv in 2019. Seasonal oscillation of the atmospheric CO_2 is ubiquitous, that is more prominent in the northern hemisphere than that of the southern hemisphere (Keeling *et al.* 2005; Jiang *et al.* 2016; Imasu and Tanabe 2018). Oscillations of the atmospheric CO_2 at intra-seasonal and inter-annual scales have been discussed in numerous studies (Li *et al.* 2010; Jiang *et al.* 2013; Li *et al.* 2018). These changes and variability in the atmospheric CO_2 could be explained as the response of the atmosphere to the inputs from anthropogenic and natural processes over the continents and oceans (Keeling *et al.* 2005; Hungershoefer *et al.* 2010; LeQuéré *et al.* 2018). Emissions from the fossil fuel combustion and land-use changes are two major anthropogenic sources, which contribute almost 7 PgC annually to the atmosphere. Terrestrial ecosystems and oceans are two major sinks; together, they are responsible for removing half of the CO_2 content that enters into the atmosphere annually through the anthropogenic emissions (Raupach *et al.* 2007). The uptake by terrestrial ecosystems is due to an increase of the primary production (photosynthesis) over the respiration and other oxidative processes (decomposition or combustion of organic material). Land-use changes (particularly deforestation) could lead to a loss of carbon from the plants and soils, which leads the terrestrial systems turn out to be an anthropogenic source of CO_2 (Houghton and Goodale 2004).

Temporal dynamics of atmosphere CO_2 level has strong linkage with the variability of surface fluxes and their transport within the atmosphere. Seasonal cycle of the atmospheric CO_2 is driven by the seasonal cycle of the weather conditions and associated CO_2 exchange by the terrestrial ecosystem (Idso *et al.* 2000). On the other hand, the large-scale disturbances of the terrestrial ecosystems associated with extreme climatic events such as flood, drought and forest fires found as the causes of the inter-annual variability (Francey *et al.* 1995; Keeling *et al.* 1995; Zimov *et al.* 1999; Jiang *et al.* 2010; Keenan *et al.* 2016). Climatic variability and its fluctuations such as the El-Niño Southern Oscillation (ENSO) have significant influence on the inter-annual variability (Dettinger and Ghil 1998; Rayner and Law 1999). During the El Niño (La-Niña) events, atmospheric CO_2 concentration increases (decreases) due to decline (enhancement) of terrestrial productivity accompanied with enhancement (decline) of soil-respiration (Jones *et al.* 2003a, b) and reduction (enhancement) of oceanic release due to weakening of coastal upwelling events in the tropical oceans (Feely *et al.* 1987). In addition to these large-scale variabilities, there exist significant regional variability in the atmospheric CO_2 associated with the perturbations in the global scale phenomenon and spatial heterogeneity in the structure and functioning of the terrestrial and marine ecosystem as well as in the physiography, climate and weather system across the globe. While most of the early research tried to elucidate possible linkages between source and sink patterns associated with carbon cycle at the global scale (Tans *et al.* 1990; Fan *et al.* 1998; Gloor *et al.* 1999; Sabine *et al.* 2004), efforts have been made in the recent time to improve understanding of the carbon cycle at the regional scale through collection of accurate, high temporal and spatial measurements by setting up global networks of *in-situ* observation and satellite retrievals, and development of numerical model to integrate all these databases in to reliable information (Deng *et al.* 2014). Atmosphere transport models such as the Goddard Earth Observing System-Chemistry (GEOS-Chem) transport model were developed. Besides, data inversion models are used to estimate unknown source and sinks of CO_2 through constraining the transport model by *in-situ* and satellite observations (Tans *et al.* 1990; Fan *et al.* 1998; Gloor *et al.* 1999).

India is a tropical nation with monsoonal climate and weather system. It is surrounded by north tropical Indian Ocean on south, east and west, and has land extension to the north. The country has diverse landforms and vegetation covers with the forest and the cropland accounted around 21% and 55%, respectively, of the total surface area. Physiography of India has three major divisions with the Himalayan Mountain in the north, the Indo Gangetic Plain in the central and the peninsular plateau in the south which includes the coastal plain and group of islands. Seasonal reversal monsoon winds prevail southwesterly during the summer and northeasterly during the winter. India receives about 75% of its total annual rainfall

during the summer monsoon period, June–September (Parthasarthy 1984; Gadgil *et al.* 2006; Ghosh *et al.* 2016). The monsoon winds have significant influence on the circulation of the north tropical Indian Ocean (Schott and McCreary 2001). The monsoon climate with a significant spatial and temporal variability is responsible in shaping the distinct patterns of sink and source of atmospheric CO_2 over India. Nayak *et al.* (2015) have shown that the terrestrial ecosystem of India behaves as a net sink of atmosphere CO_2 during 1981–2006 with mean annual Net Ecosystem Productivity (NEP) budget of 20 TgC which has significant seasonal and inter-annual variability. Results from the inverse model studies of atmospheric CO_2 over south Asian region have shown the similar characteristics about the Indian terrestrial ecosystem (Cervarich *et al.* 2016). Studies have shown that the Arabian Sea and the Bay of Bengal were described as perennial source of atmospheric CO_2 and respectively they export +64 and +13 TgC annually to the atmosphere (Bates *et al.* 2006; Valsala and Maksyutov 2013; Sarma *et al.* 2013). Analysis of *in-situ* and satellite observations have shown that monsoon and associated atmosphere transport have significant influence on the seasonal patterns of tropospheric CO_2 variability over India (Tiwari *et al.* 2014; Krishnapriya *et al.* 2017). However, a detailed budget study for quantifying contributions of various processes at work on the control of seasonal cycle and annual tendency of the atmospheric CO_2 over India yet to be carried out, which form the scope of our study. To answer this, we use GEOS-Chem model diagnostic solutions to quantify the budget of CO_2 tendency at seasonal and annual time scales, and associated contributions from different processes. Prior to this, simulated CO_2 concentration and tendency (time rate of change) of the model output were evaluated by comparing with GOSAT retrievals and *in-situ* measurements from a global view and two ISRO-flux tower stations.

2. Data and method

2.1 *Model simulations*

The physical basis and applications of the GEO-Chem model is described in detail in numerous studies (Bey *et al.* 2001; Suntaralingam *et al.* 2004; Nassar *et al.* 2010). The governing equation of the model is based on conservation of mass in which the advection scheme is parameterized on the Flux Form Semi-Lagrangian scheme (FFSL) developed by Lin and Rood (1996) and the moist convective mixing scheme of Allen *et al.* (1986). In this study, we used the 9-02 version of GEOS-Chem atmospheric transport model at 2°×2.5° spatial resolution in a regular latitude–longitude grid and 47 pressure levels along the vertical, extended from 1006 to 0.01 hPa, to simulate tropospheric CO_2 over the globe at 3-hourly intervals for the period 2006–2015. Mean vertical profiles of CO_2 at daily time-scale were stored for the study period along with various diagnostic terms, i.e., contributions of various processes such as zonal, meridional, and vertical transports, convection and eddy diffusive processes, for the analysis. The model is driven by GEOS assimilated meteorological fields and input fluxes of CO_2 from various natural and anthropogenic processes. Nassar *et al.* (2010) developed a procedure to integrate all these data into the GEOS-Chem modelling system. The data of anthropogenic CO_2 emissions were composed of cement production and fossil fuel burning based on the monthly inventory database (with 1×1 degree spatial-grid) from Carbon Dioxide Information and Analysis Centre (CDIAC) of the Oak Ridge National Laboratory (ORNL) for the years 2006–2009 and from Open Data Inventory for Anthropogenic CO_2 (ODIAC) project of National Institute for Environmental Studies (NIES), Japan for the years 2010–2015. It is noteworthy that the ODIAC database has been extrapolated from CDIAC database for the recent years starting from 2010 at high-spatial-resolution 1×1 km (Oda *et al.* 2018). The annual mean biofuel emission data used in this study was developed by Yevich and Logan (2003). Data of CO_2 emission from biomass burning was taken from Global Fire Emission Database version 3 (GFEDV3; Van der Werf *et al.* 2006). The data of air-sea CO_2 fluxes at monthly scale were used from Takahashi *et al.* (2009) that have nonzero long-term (annual) mean and null inter-annual variability. The data of terrestrial ecosystem CO_2 fluxes, known as net terrestrial exchanges (NTE), were based on Carnegie-Ames-Stanford-Approach (CASA) model (Potter *et al.* 1993) output for the 'balanced biosphere' condition, which has zero long-term (annual) mean, and null inter-annual variability. Thus, the residual inter-annual component of the air–sea fluxes of CO_2 and long-term mean and inter-annual component of the NTE were taken from the inverse modelling of 'TransCom 3' project (Baker *et al.* 2006). TransCom

3 used Bayesian synthesis inversion to estimate CO_2 source and sink over 22 predefined emission regions across the globe over oceans and continents given a set of atmospheric concentration data (from 78 global view stations and 22 flux) constraining the monthly ensemble of 13 atmospheric transport model output as the priority. These CO_2 flux inversion at monthly scale were decomposed into long-term mean, seasonal cycle and inter-annual component through posterior error covariance analysis.

2.2 *Observations*

We used the data of atmospheric CO_2 concentration from the Greenhouse gases Observing Satellite (GOSAT) of Japan Aerospace Exploration Agency (JAXA) corresponding to the short-wave infrared (SWIR) Level-3B columnar CO_2 data product (GOSAT-L3B) and Level-4B CO_2 concentration at different level of the atmosphere (GOSAT-L4B). The GOSAT is in operation since January 2009 that has been measuring atmospheric CO_2 concentration across the globe along with other trace gasses (Kuze *et al.* 2009; Yokota *et al.* 2009). It has carried the main observation instrument unit Thermal And Near infrared Sensor for carbon Observation (TANSO) which consists of Fourier Transform Spectrometer (FTS) and Cloud and Aerosol Imager (CAI). The FTS measures the solar radiation reflected from the ground by the sensor at three SWIR bands (0.76, 1.6 and 2.0 μm) and the ground and atmospheric radiation at a wide thermal infrared (TIR) bands (5.5–14.3 μm). These allow retrieval of CO_2 along with CH_4, H_2O and O_2. The SWIR bands are more sensitive to the surface layer CO_2 concentration, while the TIR bands are more sensitive to the middle and upper tropospheric CO_2 concentration (Yoshida *et al.* 2011). The CAI imageries were used for screening the FTS spectral measurements. The cloud screened pixels of the FTS SWIR radiance spectra were used to retrieve Level 2 XCO_2 corresponding to the column averaged CO_2 dry air mole fraction (Yoshida *et al.* 2013). These data products were interpolated by kriging procedure and converted into FTS SWIR Level-3, GOSAT-L3B monthly columnar product at 2.5°×2.5° over the globe (Watanabe *et al.* 2015). The GOSAT-L4A data products are surface fluxes of CO_2 inferred from dry air mole fraction of CO_2 retrieval from GOSAT-L1B radiance spectra and the ground-based measurements from GLOBAL-VIEW (NOAA-ESRL) stations through a data inversion model (Takagi *et al.* 2014). The GOSAT-L4B data product of atmospheric CO_2 concentrations were simulated over the globe at 17 vertical levels and at 6-hourly temporal intervals through a forward transport model driven by GOSAT-L4A surface fluxes in a spatial grid of 2.5°×2.5°. These GOSAT-L3B, GOSAT-L4B and GOSAT-LA data products for the period January 2010–December 2015 were archived from the GOSAT project of National Institute for Environmental Studies (https://data.gosat.nies.go.jp).

The *in-situ* observations of surface layer CO_2 used in this study are based on the measurements at Cape Rama GLOBAL-VIEW monitoring station for the period during 2009–2012, and flux tower stations at the Sundarban forest reserve for the period 2012–2013 and the Betul forest reserve for the year 2013 in the Indian subcontinent (figure 1). The Cape Rama is a maritime site located in the south of Panaji, on the west coast of India. This station is devoid of vegetation from all sides and is highly influenced by monsoon winds (Bhattacharya *et al.* 2009; Tiwari *et al.* 2011; Bhuvanachandra *et al.* 2016). During the south-west monsoon, the site receives air masses coming from the oceanic region and shows strong marine signature while the air-masses measured during the north-east monsoon period have continental signature.

Betul and Sundarban eddy covariance flux towers were installed under National Carbon Project of ISRO-Geosphere-Biosphere Programme (ISRO-GBP) with specific aim to capture the local vegetation responses in the atmospheric CO_2 measurements. Betul flux tower is located inside a deciduous forest area, with the dominance of teak tress, in Madhya Pradesh in central India which is at 507 m above the sea level. The flux tower has been set up on October 2011 at a height of 34 m, where the average height of the canopy is 22 m. It is equipped with slow and fast response sensors at various heights. Fast response sensors measure CO_2, H_2O and heat fluxes at a frequency of 10 Hz using eddy covariance based open path Infrared Gas Analyzer (IRGA-LICOR7500) and 3D Ultrasonic Anemometer (RM Young81000) at temporal scale of 30 min. Similarly, slow response sensors measure meteorological parameters like wind speed and direction, air temperature, etc. The detailed description about the data processing, flux calculation and calibration/validation procedure were given in Jha *et al.* (2013) and Rodda *et al.* (2016). The Sundarban Flux tower is operational since 1 April 2012 with the similar kind of instrumentation as that of the Betul. This is a 15-m tower inside a

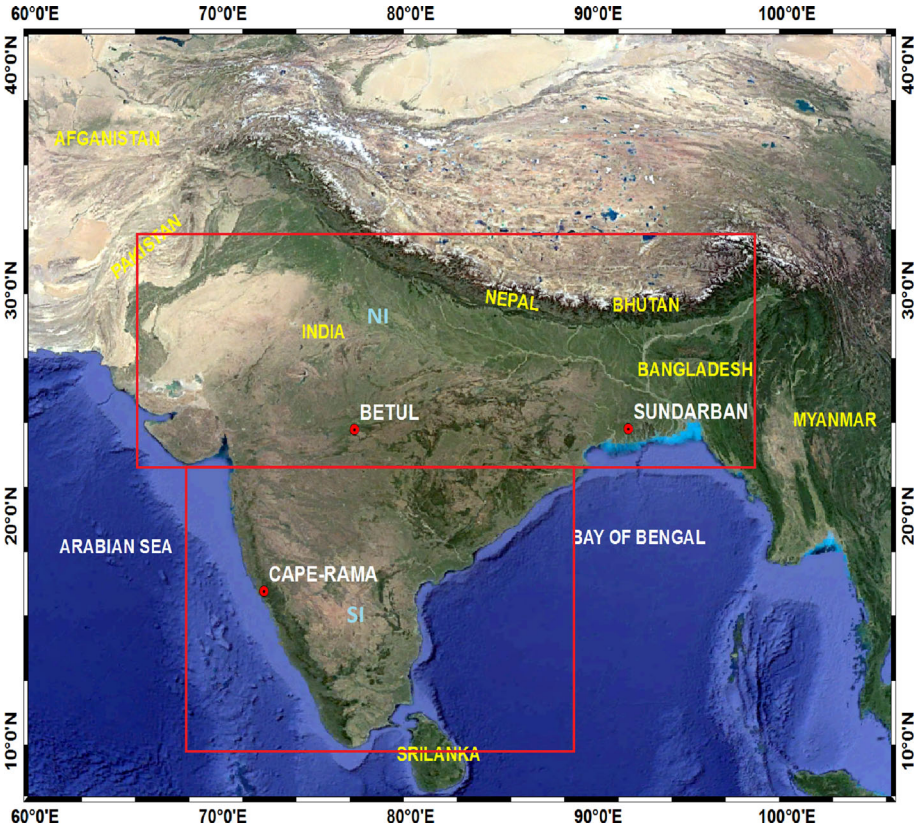

Figure 1. The study region shows the natural vegetation covers highlighting the location of GLOBAL-VIEW flux tower station at Cape Rama in the west coast of India and two ISRO flux tower stations at Betul in the central India and Sundarban in the West Bengal state of India, and two bounding boxes representing the regional domains in north India (NI) and south Indian (SI) for which specific budget analysis were carried out in this study. The map is created from https://www.google.com/maps.

mangrove patch located in the Ganges–Brahmaputra delta, in West Bengal State of India, approximately 7 m above the sea level with an average canopy height of 5 m. It is worth noting, the Sundarban is the largest continuous mangrove forest in the world, approximately 7% of the global mangrove area, spreads across 34% in Indian Territory and 66% in Bangladesh (Mukhopadhyay *et al.* 2002; Biswas *et al.* 2004; Rodda *et al.* 2016). Additionally, this tower is equipped with sensors measuring photosynthetic active radiation (PAR), air temperature, humidity, net radiation, soil heat flux, soil temperature, etc. Detailed description of data processing, calibration methods and standard corrections used during the estimation of these parameters can be found in Rodda *et al.* (2016).

2.3 *Estimation of CO_2 tendency, model diagnostics and seasonal harmonics*

The mass conservation equation of atmospheric CO_2 in a unit grid element of the study region can be expressed as:

$$\left[\frac{\partial\bar{\rho}\bar{\chi}}{\partial t}+\nabla_h.\bar{\rho}\,\overline{U_h}\bar{\chi}+\frac{\partial\bar{\rho}\bar{w}\bar{\chi}}{\partial z}+\nabla_h.\bar{\rho}\,\overline{U_h'\chi'}+\frac{\partial\bar{\rho}\,\overline{w'\chi'}}{\partial z}\right]dV - \bar{Q}dS=0, \quad (1)$$

where the subscript h refers to horizontal vectors, ρ is the density of air mass, χ is the mass mixing ratio of CO_2; U_h horizontal component of velocity and w is the vertical component of the velocity. The bar and prime notations, respectively, represent the mean state and the perturbation (temporal fluctuation) associated with various state parameters involved in the equation.

The first term in the left-hand side of the equation is the tendency of CO_2, the second and third terms, respectively, represent transport of CO_2 associated with horizontal and vertical advection processes, the fourth term represents horizontal diffusion, the fifth represents the effect of the unresolved scales along the vertical, composed of diffusion and convection processes, and the sixth term (Q) represents surface fluxes of CO_2 (at the air–sea or land–atmosphere interfaces). As described in section 2.1, the GEOS-Chem solves

the equation in a reduced pressure coordinate system at each grid element of volume dV enclosed in the surface area element dS with elemental length dx along the longitude, elemental breadth dy along the latitude and height element dz (corresponding pressure element dp).

Contributions of various diagnostics processes of the CO_2 tendency term were estimated at a daily interval in order to perform budget analysis in section 3. All these terms were integrated over the time and translated into the unit of kg and then converted into the unit of mass mixing ratio by dividing air mass (ρdV in kg) of the grid element. These were then converted to the volume mixing ratio by multiplying the ratio of the mean molecular weight of air and molecular mass of CO_2, i.e., 28.97/44.01 (g/mole). These data were translated into the unit of 'ppmv' for analysis in the next section. It is noteworthy to state that the surface flux term is implicitly included in the vertical diffusion as the surface boundary condition in the model, and is not considered separately for the analysis. We have shown the comparison between the modelled vertical diffusion tendencies and observed surface flux of CO_2 in figure 2. Both data show a good agreement between them with a negative phase (decreasing) during September–March and a positive (increasing) phase during April–August.

In section 3.2, the comparison between the simulated surface layer CO_2 and *in-situ* observation was performed in two different units: one in volume mixing ratio χ_v (in ppmv) and other in mass density (mass per unit volume). It is because, the original measurement at the flux tower stations were made in units of milli moles m^{-3}, and the temporal dynamics of atmospheric CO_2 follows mass conservation principle rather than the volume conservation, as the air is highly compressible. Following to the Avogadro's equation of gaseous volume and ideal gas equation, atmospheric CO_2 concentration in ppmv can be estimated from the units of mole m^{-3} through the transformation: $\chi_v = \left(\frac{\rho_{CO_2} \times 22.4}{10^6}\right)\left(\frac{T}{300}\right)\left(\frac{1}{P}\right)$, where, ρ_{CO_2} is observed CO_2 concentration in moles m^{-3} at T K temperature and P in standard atmospheric pressure. The above expression was used in this study to convert data from one unit to another. Since the *in-situ* data at the flux tower station contained high frequency variability, we converted them into weekly data using simple averaging procedure, then time rate of change, i.e., tendency has been estimated. The same procedure was followed for the model dataset. In

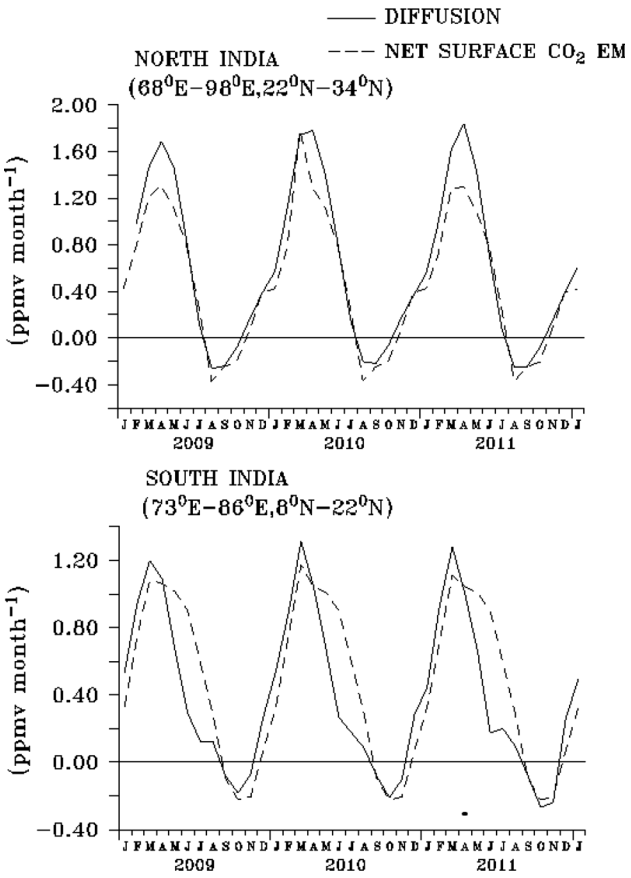

Figure 2. Comparison between the integrated surface layer CO_2 tendency (up to 690 hPa) associated with turbulent (diffusion) fluxes (solid line) and net surface CO_2 fluxes (dashed line) over north India (upper panel) and south India (lower panel), respectively. Net surface CO_2 fluxes are estimated by adding anthropogenic emissions like fossil fuel emissions and cement production, biomass burning, and net ecosystem exchanges.

section 3.3, we estimated budget for the lower troposphere by averaging the contributions from each grid boxes for entire air-column, and for the air column up to 690 hPa ($\sim$3.1 km) in order to compare with satellite retrieval and to understand the variability of CO_2 tendency in relation to various governing processes. The tendency term was expressed in units of ppmv $month^{-1}$, both for model analysis and observations. The simulated tendency is estimated from the simulated field of CO_2 mixing ratio (χ_{sim}), and the observed tendency from the observed CO_2 mixing ratio (χ_{obs}) combining with GEOS simulated density of air mass (ρ_{sim}).

We adopted least square error optimization procedure based on harmonic analysis to decompose the time series of tropospheric CO_2 tendency (and associate contributions) into annual and semi-annual harmonics and climatological mean

following to Nayak *et al.* (2016) for synthesis of mean seasonal cycle in section 3.3. Let $A(t)$ be the time series that can be expressed as:

$$A(t) = A_0 + A_1 t + A_a \cos(w_a t + \Phi_a) + A_{as} \cos(w_{as} t + \Phi_{as}) + e. \quad (2)$$

Here A_0 is a stationary component that represents the climatological mean; A_1 represents the slope of the linear trend line of the parameter with respect to time t; (A_a, A_{as}) and (Φ_a, Φ_{as}) denote amplitude and phase angles of annual and semi-annual harmonics, respectively; e represents residual term and the white noise.

3. Results

3.1 *Spatial and temporal patterns of zonal mean CO_2 as simulated by GEOS-Chem*

The important modes of the observed large-scale distribution patterns of the CO_2, as discussed in earlier studies, are the existence of strong seasonality and gradients along the latitudinal and the altitudinal directions (Miyazaki *et al.* 2008; Diallo *et al.* 2017). Thus, GEOS-Chem model simulations were analyzed in figure 3 to examine its consistency with the above observed finding. The latitude-vertical cross-section of the zonal mean (60°–100°E) atmospheric CO_2 concentration and vertical velocity (from the surface at 1000–10 hPa pressure level) in the extended study region along the latitude (40°S–40°E) during four seasons of a year is shown in the figure. It reveals that tropospheric CO_2 in the northern tropics has higher concentration during winter (December–February) and spring seasons (March–May) together with updraft of enriched CO_2 from lower to the upper troposphere (as inferred from negative contours in the figure). During summer monsoon (June–August) and autumn (September–November), CO_2 concentration decreases/depleted throughout the atmospheric column together with an updraft of air-parcel. Diallo *et al.* (2017) described this declining of CO_2 in the northern tropics is mainly due to uptake of CO_2 by the terrestrial ecosystem. In contrast to the distribution of CO_2 in the northern tropic, the troposphere in the southern tropics exhibits stratified CO_2 with higher values in the upper level than the lower level throughout the year. This along with the downward velocity (downdraft) indicates the subsidence of atmospheric CO_2 which implies that oceanic regions have been playing a key role on the uptake of atmospheric CO_2. The seasonality of CO_2 concentration is more prominent in the lower troposphere up to 200 hPa (8 km) than the upper troposphere. These variations could be attributed to the influence of seasonal variations of the surface fluxes of CO_2 and atmospheric transport processes (Miyazaki *et al.* 2008; Diallo *et al.* 2017).

3.2 *Comparing model simulations and observations*

Figure 4 shows comparison between simulated CO_2 and *in-situ* observations at Cape Rama global view station and Betul and Sundarban flux tower locations. Comparison has been performed in three different ways: in two different units of concentration level such as volume mixing ratio in ppmv and mass density in milli moles m^{-3} and tendency. The tendency refers to the time rate of change of CO_2 content of the surface layer which has been estimated at each of the observation station using the procedure given in section 2.2.

The Cape Rama site is located on the west coast of India. As already described, this station is away from the anthropogenic sources and comes under the influence of seasonal reversal of winds of the monsoon. Thus, associated variability of the measured CO_2 is expected to be influenced primarily by monsoonal transport and secondarily by local vegetation processes (Tiwari *et al.* 2011; Bhuvanachandra *et al.* 2016). The concentration values as shown in figure 4(a) corresponding to ppmv unit and in figure 4(b) for milli mole m^{-3} units, exhibit the similar seasonal cycle, and linear increasing rate for model and observations. Please note that, a bias of 5 ppmv was subtracted from the observed data for the comparison in figure 4(a) and associated corrections were made in figure 4(b). However, the model has significant differences from the observation in its inter-annual variability, especially for the year 2012. In this year, observation station noticed a large amplification of the CO_2 level along with one-month phase lag than the earlier years, 2010 and 2011. This can be attributed either to the data uncertainty or the influences of strong La-Niña effect. On the other hand, the model does not show such variability. The La-Niña is the negative phase of El-Niño Southern Oscillation (ENSO) events and opposite to the El-Niño phase; and 2011–2012 years witnessed strong La-Niña event, which usually influences the

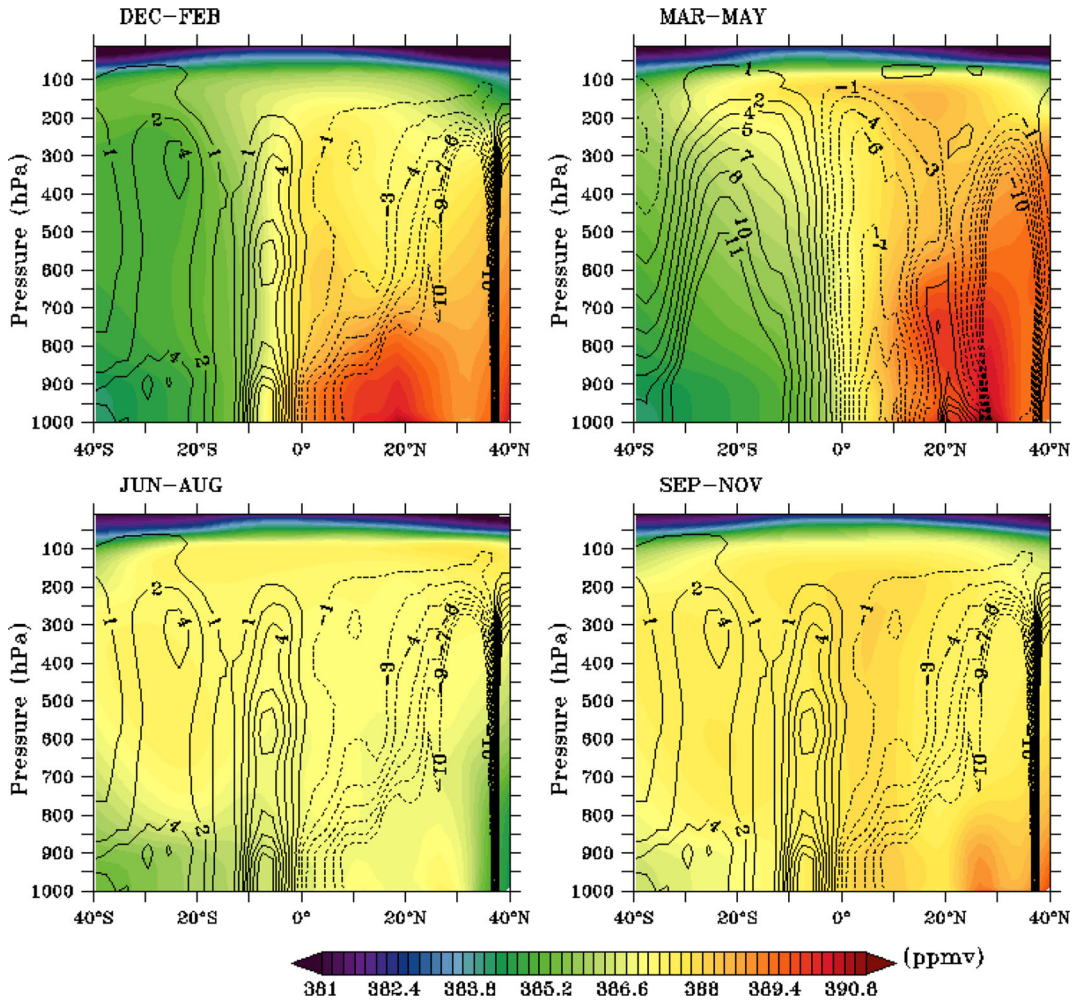

Figure 3. Latitude–pressure distribution of seasonal climatology of simulated zonal mean over (60°–100°E) CO_2 in ppmv (shaded colours) and vertical velocities ($\times 10^{-3}$) in Pa/s (contour lines) based on GEOS-Chem model are shown. The negative contour (dotted lines) represents the upward movement of air parcels, and the positive contour (solid lines) represents the downward movement of air parcels.

circulation and weather patterns across the globe with favoured and good rainfall conditions over India. However, further investigation is beyond the scope of present study. In figure 4(c), the model tendency of mass density shows overall agreement with the observed tendency with well-marked coherent seasonal cycle with negative (decreasing) phase during May–September and a positive (increasing) tendency during October–April. The correlation coefficient between these data is 0.87 (well within the range of 0.736–0.928 corresponding 95% confidence level) and they vary between the minimum value 388 ppmv (16.3 milli mole m^{-3}) and maximum value 408 ppmv (17 milli mole m^{-3}) with mean amplitude of seasonal cycle is 4.5 ppmv (0.25 milli mole m^{-3}).

The measurement corresponding to flux towers were planned to capture the signals of local vegetation activity, i.e., net terrestrial ecosystem exchange from a footprint of 5–10 km diameter. The flux tower observation at Sundarban site shows a significant seasonal variation of CO_2 during April 2012–March 2013. The observed concentration in ppmv as shown in figure 4(d) shows a decreasing trend during spring (February–March 2013) and summer (April–August 2012) seasons, and increasing trend during in autumn and winter (September–December 2012). The summer time decreasing trend has mean value 370 ppmv which has undergone a large fluctuation with standard deviation of 20 ppmv. The model, however, show less agreement with the observation with significant deviation to produce summer time dip and a phase lag of 1–2 months. On the other hand, the comparison between the data in their mass density unit (moles m^{-3}) shows relatively

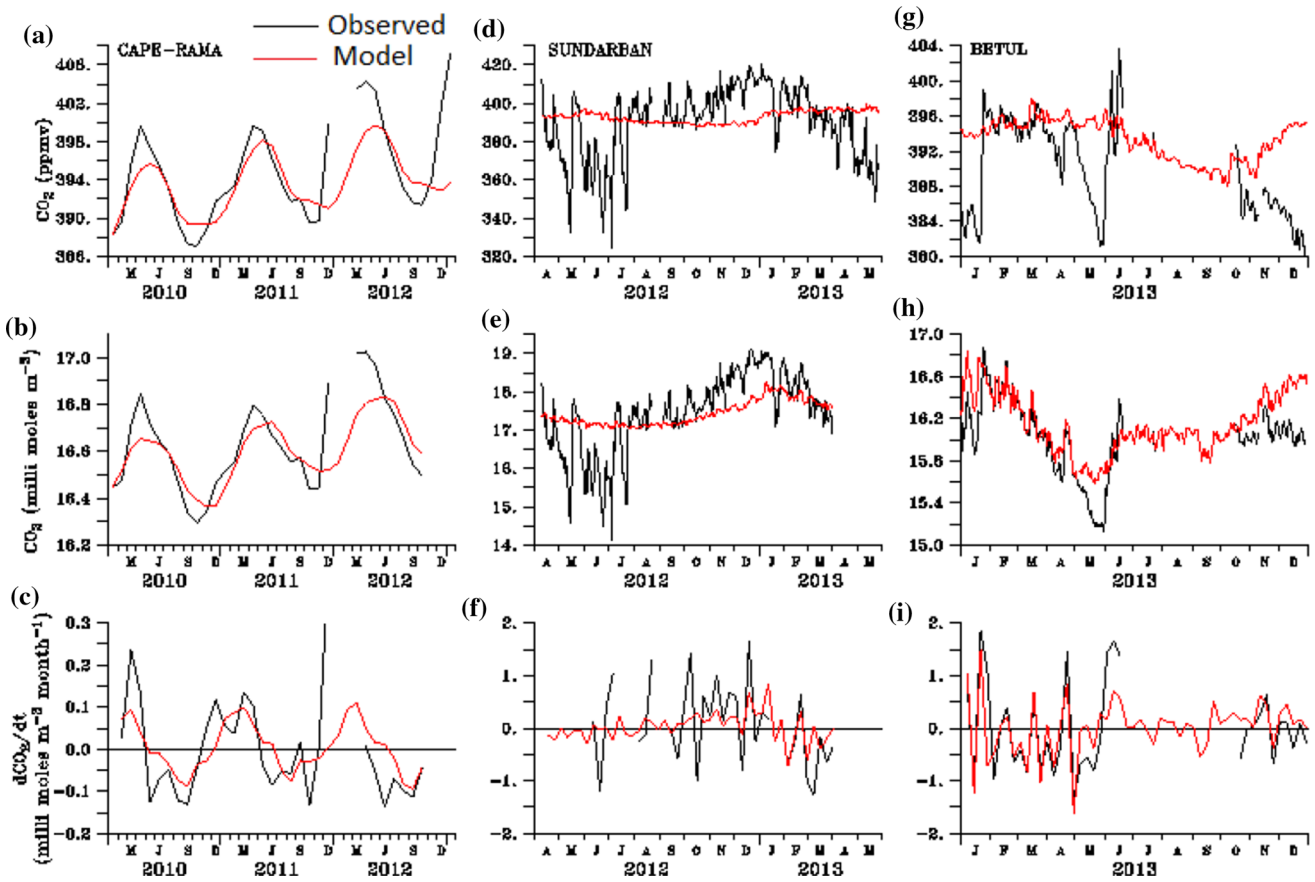

Figure 4. Left panels (**a–c**) show comparison between *in-situ* and simulated near surface layer atmospheric CO_2 at Cape-Rama GLOBAL VIEW station in ppmv (upper panel), in milli mole m^{-3} in middle panel, and tendency in milli mole m^{-3} $month^{-1}$ in the bottom panel. The middle panels (**d–f**) show the same as that in the left panels, but for Sundarban flux tower station and the right panels (**g–i**) show the same as that in the left panels, but for Betul flux tower station.

better agreement (figure 4e). They coherently exhibit a distinct seasonal cycle dominated by annual oscillation with increasing phase during June–December and decreasing phase during January–April. However, the model still has a significant deviation to reproduce summer time dip. The comparison between the data in their time rate of change of mass density (tendency) form in figure 4(f), shows an overall agreement in their high-frequency (weekly) oscillation with negative tendency during April–August (however, with a strong oscillatory signal in observed tendency) and during February–March 2013, and positive tendency during September–December 2012. Please note that, a band-pass filter has been used in the figure to remove the signal more than 2 units or < -2 units in the observed data. It has correlation coefficient 0.71 for the sample size of 42 (excluding the missing data points) and well within the interval 0.518–0.833 corresponding to 95% confidence level. Earlier, Rodda *et al.* (2016) attributed the summer time reduction along with the significant fluctuation (standard deviation) in the observed data as the response of the ecosystem uptake of the local vegetation associated with significant fluctuation in availability of photosynthetic radiation during cloudy or rainy days. However, the model has missed this signal, which might be due to its coarse nature to capture the local signature.

Figure 4(g–i) shows comparison between the model and observation for the Betul flux tower station which is located in the central India within the deciduous forest dominated by teak trees (Jha *et al.* 2013). The simulated CO_2 concentration level in ppmv shows over all good agreement with the *in-situ* observation, but with a significant difference for the period during the late autumn and following winter season, October–December 2013, and January 2013 in figure 4(g). In this period, the model exhibits increasing trend in contrast to the decreasing trend in the observation. In addition to this, the observation shows a dip during April–May 2013, that is absent in the

simulated data. On the other hand, the comparison between the data in their mass density unit (milli moles m^{-3}) as shown in figure 4(h) shows very good agreement between them with correlation coefficient 0.88, which is well within the 0.788–0.933 at 95% confidence level for 38 non-missing data points. They exhibit distinct seasonal cycle with decreasing value during February–May 2013, remain uniform during June–August 2013, a short time decreasing trend during September and then increasing trend during October–December 2013. This kind of variability of the seasonal cycle with one primary decreasing phase along with secondary decreasing phase with increasing phases in-between is the uniqueness about the region and is referred as the semi-annual oscillations of the near surface atmospheric CO_2 variability due to the response of the local vegetation activity. These short duration increasing phases in measured CO_2 tendency can be attributed to the decline of ecosystem uptake processes owing to the leaf dehiscence of deciduous vegetation in the study region (Jha *et al.* 2013); while the decreasing phases of relatively longer duration have good association with the regional vegetation uptake and transport processes. The ecosystem in this region acted as CO_2 sink during the winter season, while very less CO_2 fixation is observed during the summer. The comparison between the data in their tendency of CO_2 mass density in figure 4(i) shows very good agreement with coherent high-frequency oscillations in their weekly data on the background of mean negative tendency during February–May 2013 and either positive or negligible tendency during June–December 2013.

3.3 *Comparison of modelled CO_2 tendency with satellite observation*

Figure 5 shows a comparison between simulated tropospheric columnar (mean) CO_2 concentration (tendency, i.e., time rate of change of CO_2) and GOSAT L3B observation (tendency) for the north and south sub-regions of India. North India is comprised of the cropland dominance Indo-Gangetic plain, high altitude evergreen forest and snow cover regions of the Himalayan Mountain, and grassland dominance of Rajasthan and Gujarat that includes the Thar Desert. North India is relatively away from the marine environment and has been characterized by subtropical continental climate. On the other hand, southern peninsular India comes under the influence of marine environment, which comprises Western Ghats with evergreen trees, central plateau covered by grassland and deciduous forest, and cropland dominated eastern plains (Jain *et al.* 2007). As shown in the left panels of figure 5, modelled CO_2 concentration corresponding to the lower tropospheric columnar mean has better agreement with the GOSAT observation than that of the total atmosphere columnar mean. This result is quite expected as the SWIR band of the GOSAT is more sensitive to the surface layer CO_2 concentration level and less sensitive to middle and upper tropospheric CO_2 concentration (Yoshida *et al.* 2011). However, both data show the similar range of concentration between 384 and 400 ppmv and a distinct seasonal cycle, inter-annual variability and positive linear growth rate (approximately 2 ppmv yr^{-1}) during the study period. In terms of tendency in the right panels of figure 5, it exhibits a positive phase (corresponding to an increasing trend of CO_2 concentration) during September–March and a negative phase (CO_2 decreasing trend) during April–August. However, the general trend of annual evolution of the lower tropospheric CO_2 tendency is similar for both the regions. They show a significant difference in terms of their seasonal amplitudes, variability and relative contributions of various diagnostic processes of net tendency.

Figure 6 shows the synthesized time series of mean seasonal cycles both for observation and model CO_2 tendency using the procedure discussed in section 2.3 (equation 2) for north India and south India. The seasonal cycle of north India has a bi-annual oscillation with a primary peak (at 1.5 ppmv $month^{-1}$) in October; a secondary peak (at 1.25 ppmv $month^{-1}$) in February; a primary trough (-2.5 ppmv $month^{-1}$) in June and a secondary trough (0.75 ppmv $month^{-1}$) in December. This bi-annual oscillation is prominently seen in the model, however, relatively less in satellite observation. *In-situ* observation at the Betul flux tower (located in the central India) discussed in earlier section exhibited similar signature of semi-annual oscillation. On the other hand, the bi-annual oscillation in case of south India is less apparent in the satellite observation as well as in the model; it mostly follows an annual oscillation with a single peak in October (2 ppmv $month^{-1}$) and a single trough in June (-3 ppmv $month^{-1}$). The mean amplitude of the seasonal oscillation of

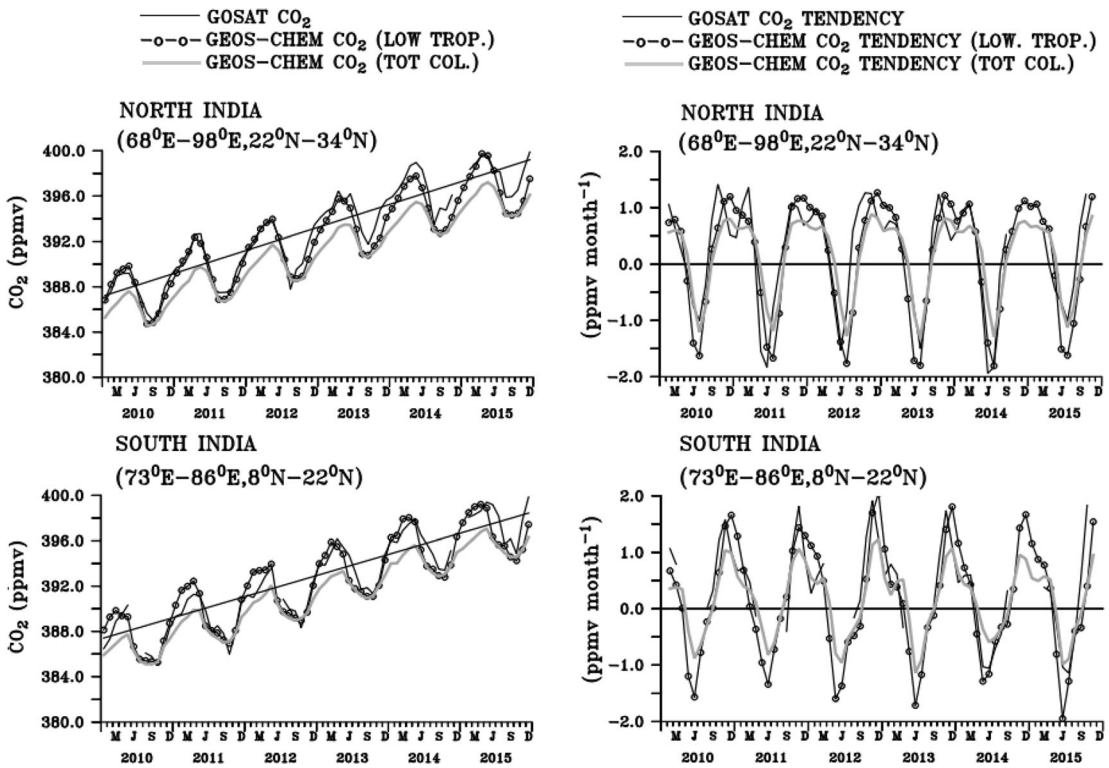

Figure 5. The left panels show the comparison of simulated mean CO_2 corresponding to the lower troposphere (circled line) and total atmospheric column (grey continuous line) with GOSAT observation (black continuous line) for the northern (upper panel) and southern (lower panel) domains of India. The right panels show the comparison among their respective tendencies. The CO_2 concentration is expressed in the unit of ppmv and tendency is expressed in ppmv month^{-1}.

north India during the positive phase of CO_2 tendency (October–March) is relatively lower than the amplitude of south India. The decreasing CO_2 tendency over north India can be attributed to a strong drawdown of CO_2 by the terrestrial vegetation during the summer monsoon months and following autumn season on the positive background of horizontal and vertical transport process. On the other hand, the post-winter and spring season high values can be associated with dominating effects of soil respiration and anthropogenic release over the photosynthesis. Some of the global studies have highlighted similar impact of surface fluxes characterizing the seasonal cycle of lower tropospheric CO_2 over the northern tropical and extra-tropical continents (Kong *et al.* 2010; Cao *et al.* 2017).

Following important points can be noted about the satellite data. The GOSAT-L3B has high level of uncertainty in estimating the seasonal cycle for south India due to missing data points, especially during decreasing phase (March–September) that is not the case for the north India seasonal cycle. In addition to this, the satellite retrieval has relatively smaller seasonal amplitude than that of the model synthesis. To understand further, the GOSAT-L4B data was used to synthesize the mean seasonal cycle in place of GOSAT-L3B and the result is presented in figure 6. It provides better agreement between the model and GOSAT-L4B data in terms of seasonal amplitude; however, GOSAT-L4B still missed the secondary trough during October–November for north India. We believe that this trough is an important characteristic of the region, but GOSAT-L4B missed such signature; GOSAT-L3B and model could able to resolve such variability. This deficiency can be attributed to the inherent artifact and uncertainty present in the GOSAT model with input from GOSAT-L4A surface fluxes. To conform this, we have made an additional simulation using the GOSAT-L4A surface fluxes in the GEOS-Chem model by replacing GEOS surface fluxes, the result is the same as the GOSAT-L4B analysis. Thus, it has proved our hypothesis that the GOSAT-L4A data have some artifact corresponding to north India in simulating bi-annual cycle of the atmospheric CO_2.

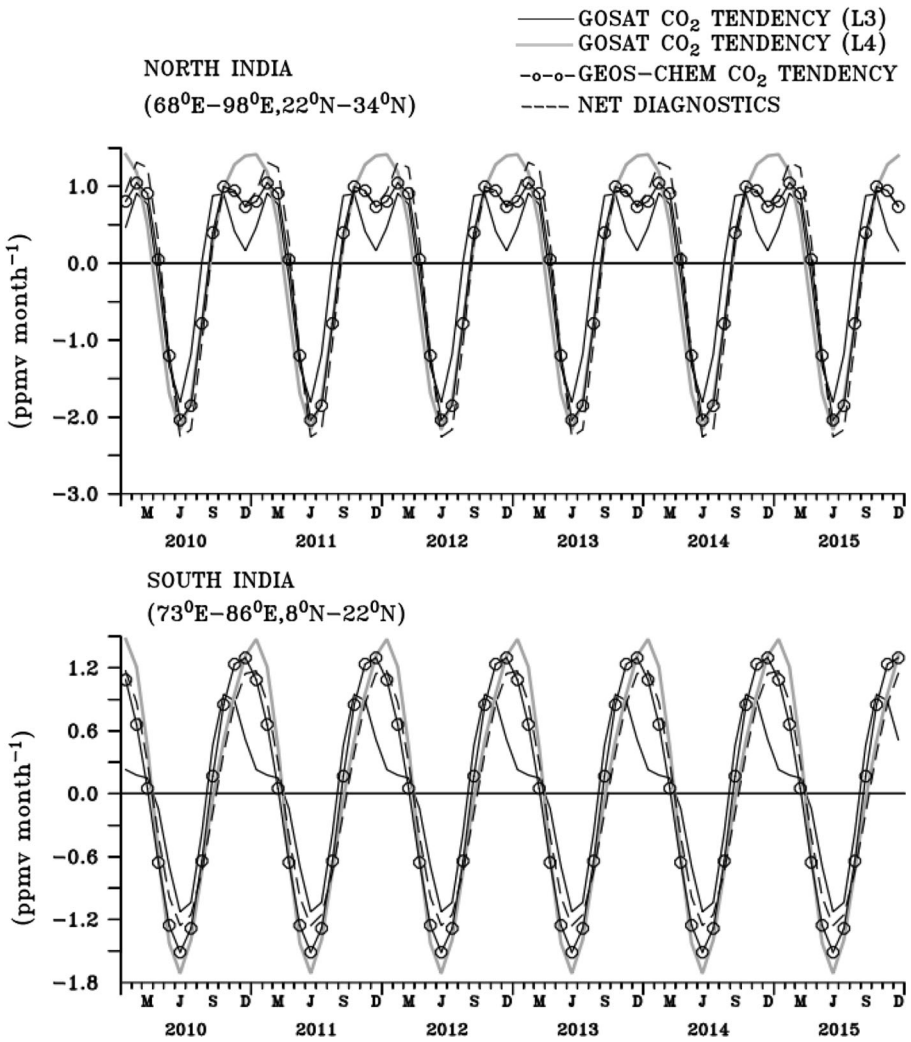

Figure 6. Mean seasonal cycle of the lower tropospheric CO_2 tendency as synthesized from the GEOS-Chem model solution (pattern line), GOSAT-L3B, and GOSAT-L4B datasets for north India in the upper panel and for south India in the lower panel. Sum of all the diagnostic (contributing) terms (as the Net Diagnostics) is also presented (as dashed line). All units are expressed in ppmv month^{-1}.

3.4 *Causes of the seasonal cycle and annual budget*

To understand causes of the seasonal cycle, we estimated budgets of different diagnostic processes associated to the CO_2 tendency of the surface layer confined up to 650 hPa with respect to major positive and negative phases. Analysis was carried out separately for north India, south India and also their area weighted mean for total India. For making ease, we re-grouped contributions of all diagnostic processes into three: horizontal advection (included contributions from both zonal and meridional advection components), vertical transport (included both advection and convection processes), and vertical diffusion (the sum of surface fluxes and perturbation of unresolved residual transport processes). Further, the key words such as positive and negative contributions have, respectively, been used in the following to represent the +ve sign and −ve sign of the CO_2 budgets associated to each of the processes. The positive (negative) contribution causes gain of CO_2 to the surface layer atmosphere over India (elemental volume over India), while the negative contribution causes loss (or removal of CO_2) from the surface layer. The budgets were estimated in terms of mass in kgC month^{-1}, and normalized to unit volume, then converted to equivalent unit of ppmv month^{-1} using simply multiplying factor presented in section 2.3. Please note that the total sum of contributing processes may differ slightly from the net tendency corresponding to ppmv scale, which is obvious due to compressibility nature of the

Table 1. *Annual budget of lower tropospheric CO_2 tendency over India and its two sub-domains: north India and south India, and associated contributions from different diagnostic processes as discussed in the text. All units are expressed in ppmv yr^{-1} (and equivalent unit GtC yr^{-1} in parenthesis) for respective regions.*

Sources/sinks	North India ppmv yr^{-1} (GtC yr^{-1})	South India ppmv yr^{-1} (GtC yr^{-1})	India ppmv yr^{-1} (GtC yr^{-1})
Horizontal advection	−13.02 (−7.56)	−6.09 (−3.54)	−9.87 (−11.10)
Vertical advection	15.81 (9.19)	8.81 (5.12)	13.67 (14.31)
Diffusion	−1.91 (−1.11)	−2.33 (−1.35)	−2.15 (−2.46)
Net surface emission	5.30 (0.36)	5.45 (0.25)	(0.61)
Net terrestrial exchange	−1.79 (−0.15)	−0.74 (−0.06)	(−1.4) (−0.21)
CO_2 tendency	0.89 (0.52)	0.38 (0.23)	(0.71) (0.75)

atmosphere (which do not follow volume conservation principle), however, these results are consistent in terms of mass unit (table 1).

The budget analysis for north India corresponding to the positive phase of net CO_2 tendency (equivalently increasing phase of CO_2 concentration) during September–March is shown in the upper left panel of figure 7. As shown, the net tendency equivalent to 0.97 ppmv $month^{-1}$ results from a positive input of 0.048 ppmv $month^{-1}$ through the horizontal advection and 0.7895 ppmv $month^{-1}$ through vertical advection, and a negative input of −0.1606 ppmv $month^{-1}$ through vertical diffusion. It is noteworthy that the vertical diffusion term in the model has included the surface fluxes of net terrestrial ecosystem (and oceanic) exchanges, anthropogenic emissions, and residual unresolved turbulence (perturbation) component. The negative contribution of the vertical diffusion process in this period includes a significant amount of terrestrial ecosystem uptake (−0.29 ppmv $month^{-1}$) and the similar amount of surface emission (0.29 ppmv $month^{-1}$). In this period, the mainland of India has been experiencing northeast monsoon winds with southwesterly horizontal components and upward vertical component. This, in combination with decreasing CO_2 concentration level from surface to higher levels (please see figure 3 for the patterns of latitude–altitude cross section of CO_2 and vertical velocity), could suggest upwelling of CO_2 enriched air-parcel leading net gain of CO_2 in the surface layer. The positive tendency of the horizontal transport during this period arises due to the advection of CO_2 enriched air-parcels from the southeast Asian region to India by northeast monsoon winds. Regarding the negative phase tendency during April–August for north India as shown in the upper right panel of figure 7, the mean tendency is −0.67 ppmv $month^{-1}$. This results from the loss of CO_2 primarily through horizontal advection (−2.86 ppmv $month^{-1}$) and secondarily through vertical diffusion (−0.15 ppmv $month^{-1}$) which dominates the gain (inward transport or positive contribution) of 1.96 ppmv $month^{-1}$ from the vertical advection. In this period, the negative contribution of vertical diffusion has included a small positive input of net terrestrial ecosystem exchange (0.03 ppmv $month^{-1}$) and a large positive input of terrestrial emission (0.565 ppmv $month^{-1}$). Unlike the positive phase, this has an intense negative contribution from the horizontal transport processes. This results from the advection of CO_2 depleted air-parcel over oceanic region to India mainly due to southwest monsoon winds (Tiwari *et al.* 2011). The positive contribution of the vertical transport and a negative contribution of vertical diffusion could be explained through the similar mechanism that had been prevailing during the positive phase of the net tendency discussed earlier.

Budget analysis of surface layer atmospheric CO_2 for south India is shown in the middle panels of figure 7. It shows the similar analysis as that of north India, but with amplified net tendency during positive phase (1.043 ppmv $month^{-1}$) as well as negative phase (−0.739 ppmv $month^{-1}$) of the seasonal cycle. The net tendency of the positive phase (September–March) results from the positive contributions (leading to the gain of CO_2 by the surface layer) of the horizontal (0.69 ppmv $month^{-1}$) and vertical (0.76 ppmv $month^{-1}$) transport processes and negative contribution of the vertical eddy diffusion (−0.13 ppmv $month^{-1}$).

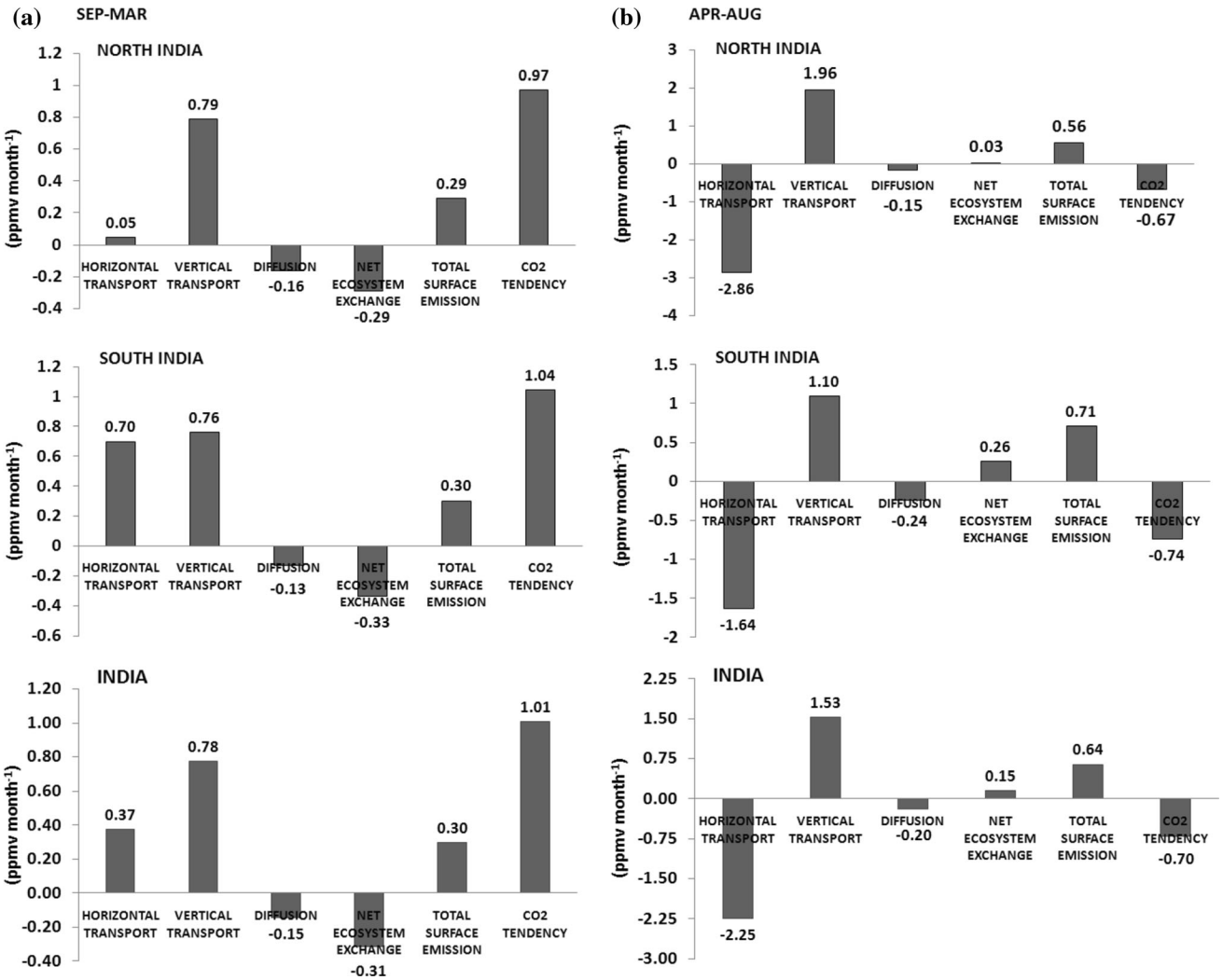

Figure 7. Analysis of CO_2 budget and associated contributions from major diagnostic processes (in ppmv month^{-1}) corresponding to the positive phase (September–March) and negative phase (April–August) of the mean seasonal cycle of CO_2 tendency over north India (upper panels), south India (middle panels) and Indian domain (lower panels) are shown in the left and right panels, respectively. The contributing terms to the net CO_2 tendency are horizontal transport (zonal+ meridional advection), vertical transport (convection + advection) and vertical diffusion (inclusive of net terrestrial exchange, net surface emission and un-resolved dynamic diffusivity). Positive numbers represent addition of CO_2 to the surface atmospheric layer and negative numbers represent loss from the surface layer. All terms are expressed in ppmv month^{-1}.

However, the vertical eddy diffusion has included -0.34 ppmv month^{-1} net ecosystem uptake and 0.30 ppmv month^{-1} surface emissions. On the other hand, the net tendency corresponding to the negative phase in April–August is mainly ascribed to the loss of CO_2 due to the horizontal transport (-1.63 ppmv month^{-1}) and vertical diffusion (-0.24 ppmv month^{-1}) that exceeds the positive tendency (1.09 ppmv month^{-1}) from the vertical advection. It is important to note that the relative sign of contributions from horizontal and vertical transport processes during the positive (or negative) phase of the net tendency over south India are the same as that of the north India. However, the major differences are the contributions coming from horizontal transport processes; which is significantly larger for south India during the positive (negative) phase as compared to reduced (enhanced) contribution for the north India.

The area weighted budget of the surface layer CO_2 over the Indian mainland, as shown in the bottom panels of figure 7, are 1.01 ppmv month^{-1} during September–March and -0.70 ppmv month^{-1} during April–August. The former results from dominant contributions of vertical advection (0.78 ppmv month^{-1}) in addition to a contribution of 0.37 ppmv month^{-1} from horizontal advection which causes excess gain of CO_2 (input) into the surface layer over a negative contribution (removal) of vertical diffusion process (-0.15 ppmv

month^{-1}). In this period, the contribution of vertical diffusion has a significant component of terrestrial ecosystem uptake (−0.31 ppmv month^{-1}) and the similar magnitude of net surface emissions (0.30 ppmv month^{-1}). The positive magnitude of vertical advection comes from upwelling of CO_2 enriched air-parcels from surface to the higher level and positive contribution of horizontal advection from the transport of CO_2 enriched air-parcels from the southeast Asian region to India by the northeast monsoon winds. On the other hand, the net tendency of the negative phase comes from the excess loss by horizontal advection (−2.25 ppmv month^{-1}) over the gain of CO_2 into the surface layer (1.53 ppmv month^{-1}) by the vertical advection in addition to a significant removal of CO_2 by vertical diffusion process (−0.20 ppmv month^{-1}). The negative contribution of horizontal transport in this period comes from transport of depleted CO_2 air parcels from oceanic region to India through the southwest monsoon winds and the positive contributions of vertical advection comes from upwelling of CO_2 enriched air-parcels from surface layer to the higher level.

At an annual scale (see table 1), lower tropospheric CO_2 budget for north India is 0.52 GtC (1 GT = 10^{12} kg) which is equivalently 0.89 ppmv yr^{-1}. This results from the amplified positive contribution of the vertical advection of 9.19 GtC (15.81 ppmv yr^{-1}) that dominated the loss of −7.56 GtC (−13.02 ppmv yr^{-1}) through the horizontal advection and −1.11 GtC (−1.91 ppmv yr^{-1}) through vertical diffusion processes. The contribution from vertical diffusion has included −0.15 GtC yr^{-1} (−1.79 ppmv yr^{-1}) from net terrestrial ecosystem uptake and terrestrial emission of 0.36 GtC yr^{-1} (5.3 ppmv yr^{-1}). Regarding south India, the net annual CO_2 tendency is 0.22 GtC yr^{-1}, equivalent to 0.38 ppmv yr^{-1}, which is less than the half of the net annual CO_2 tendency of north India. This is associated with the gain of atmospheric CO_2 by the surface layer by vertical advection 5.12 GtC yr^{-1} (8.81 ppmv yr^{-1}) that exceeds the loss, −3.54 GtC yr^{-1}, through horizontal advection (−6.0 ppmv yr^{-1}) and −1.35 GtC yr^{-1} (−2.33 ppmv yr^{-1}) vertical diffusion processes. The negative contribution of vertical diffusion in the annual budget is inclusive of net CO_2 uptake of −0.06 GtC yr^{-1} (−0.74 ppmv yr^{-1}) by the terrestrial ecosystem and 0.25 GtC yr^{-1} (5.45 ppmv yr^{-1}) terrestrial emission. The area weighted budget for Indian mainland is 0.71 GtC yr^{-1} (0.75 ppmv yr^{-1}), that is associated with the gain by vertical advection 14.31 GtC yr^{-1} (13.67 ppmv yr^{-1}) that exceeds the losses by horizontal advection −11.10 GtC yr^{-1} (−9.87 ppmv yr^{-1}) and vertical diffusion −2.46 GtC yr^{-1} (−2.15 ppmv yr^{-1}). The contribution of vertical diffusion includes 0.61 GtC yr^{-1} (5.35 ppmv yr^{-1}) surface emission and net terrestrial ecosystem exchange of −0.21 GtC yr^{-1} (−1.45 ppmv yr^{-1}). Further, the net gain of CO_2 molecule in the surface layer of atmosphere over India is 85% higher than the net input by the surface fluxes over India.

4. Summary and conclusions

On the basis of GEOS-Chem atmospheric transport model, the satellite and *in-situ* observations, we studied the seasonal variation of lower tropospheric CO_2 over India. The *in-situ* measurements at two flux tower stations, Betul and Sundarban forest reserves, represent the surface-layer CO_2 variability as the response to the regional ecosystem. The GEOS-Chem transport model has simulated a major part of the observed signal, however with some deviation. This is due to inherent uncertainty associated with the spatial resolution and input data sources as the model was built to describe the variability at a regional to the global scale. On the other hand, the model solution could successfully describe the observed seasonal variability of the lower tropospheric CO_2 at the CAPE RAMA GLOBAL-VIEW station as well as by the GOSAT-L3B columnar CO_2 over a large spatial extent.

Both GOSAT-L3B data and model analysis coherently exhibit a distinct seasonal oscillation of the tropospheric CO_2 over India with composite signal of annual and semi-annual frequency (bi-annual oscillation) for the north India and dominance of annual oscillation for the south India. The mean seasonal cycle associated with the lower troposphere has a major negative phase during April–August and a positive phase during September–March. The positive phase has a secondary trough during October–December which is more distinct in north India. The secondary trough can be explained as the drawdown of CO_2 by the terrestrial ecosystem uptake on the positive background of net tendency coming from the horizontal and vertical transport processes.

The seasonal cycle retrieved from the GOSAT-L3B for the south India suffers from an uncertainty owing to the missing data specific to the negative

phase of the seasonal cycle; however, there exist sufficient data in north India to explain the seasonal cycle. Amplitude of GOSAT-L3B mean seasonal cycle is relatively lower than the model solution. To investigate further, we used GOSAT-L4B data and performed additional GEOS-Chem simulation corresponding to GOSAT-L4A surface fluxes. The new model solution had a good agreement with GOSAT-L4B dataset and they exhibit similar mean seasonal cycle with dominance of the annual frequency, and comparable amplitude which are relatively higher than that of the GOSAT-L3B data, but nearer to the original GEOS-Chem model simulation. On the other hand, both GOSAT-L4B and new simulation have missed the secondary trough (in the autumn season), which was distinctly observed in the GOSAT-L3B and in original GEOS-Chem model simulation. This analysis has suggested that the original GEOS-Chem model solution corresponding to the GEOS surface forcing, has better regional characteristics to explain the budget of the tropospheric CO_2 over India at seasonal and annual scale.

The model diagnostics comprised of different contributing terms were analyzed to describe the major positive and negative phases of the columnar CO_2 tendency of the surface layer atmosphere within the 690 hPa pressure level. It has shown that the positive phase of the CO_2 tendency is primarily contributed by the positive contributions from the horizontal and vertical advection processes which exceed the loss (negative tendency) from vertical eddy diffusion and terrestrial ecosystem uptake. The positive magnitude of vertical advection comes from upwelling of enriched CO_2 air parcels from surface to the higher level and positive contribution of horizontal advection from the transport of CO_2 enriched air parcels from the southeast Asian region to India by the northeast monsoon winds. In this period, the contribution of vertical diffusion has included a significant component of terrestrial ecosystem uptake and the similar magnitude of net surface emissions. On the other hand, the negative phase (March–August) results from the loss (negative tendency) of CO_2 due to the horizontal advection and vertical eddy diffusion that dominated the gain (positive tendency) from the combined effect of vertical advection, terrestrial ecosystem exchanges and anthropogenic sources. The negative contribution of horizontal transport in this period comes from transport of depleted CO_2 air parcels from oceanic region to India by the southwest monsoon winds and the positive contributions of vertical advection comes from upwelling of enriched CO_2 air parcels from surface layer to the higher level.

The budget analysis for the north and south India are of similar characteristics in a broader context, with the same relative sign for contributions from horizontal and vertical transport processes. However, the major difference comes from the magnitude of the contribution by horizontal transport advection in the net tendency, which is significantly larger for south India during the positive (negative) phase as compared to reduced (enhanced) contribution for the north India.

At the annual scale, CO_2 content of the surface layer over India has a net gain of 0.75 GtC, which comes from the gain through vertical advection (14.31 GtC) that exceeds the loss due to horizontal advection (−11.10 GtC) and vertical diffusion processes (−2.46 GtC). This net gain is almost 85% higher than the net input of 0.4 GtC by surface fluxes composed of 0.61 GtC from surface emission and −0.21 GtC from net terrestrial ecosystem exchanges.

Acknowledgements

This research is carried out as part of National Carbon Project, ISRO Geosphere–Biosphere Programme executed at NRSC, Hyderabad. We are grateful to Nassar Ray, Professor, University of Toronto and the GEOS team at GSFC, NASA for providing the model support and guidance. We acknowledge the Forestry Division of NRSC, Hyderabad for providing the flux tower data. We express our due acknowledgement to various data providers such as Global view project and the GOSAT team at JAXA.

Author statement

Rabindra K Nayak perceived the idea and has taken responsibility to execute the work; M Krishnapriya played the key role on execution and involved herself completely in the research; Shaik Allahudeen and A Bhuvanachandra have contributed on the analysis of model simulations; C S Jha contributed in analysis and interpretation of *in-situ* data; S K Sasmal and K V S R Prasad have contributed in manuscript preparation and revision; V K Dadhwal and M V R Sheshasai have provided guidance throughout the research.

References

Allen D J, Rood R B, Thompson A M and Hidson R D 1986 Three dimensional ^{222}Rn calculations using assimilated data and a convective mixing algorithm; *J. Geophys. Res.* **101** 6871–6881.

Baker D F, Law R M, Gurney K R *et al.* 2006 TransCom 3 inversion inter-comparison: Impact of transport model errors on the inter-annual variability of regional CO_2 fluxes, 1988–2003; *Glob. Biogeochem. Cycles* **20** GB1002.

Bates N R, Pequignet A C and Sabine C L 2006 Ocean carbon cycling in the Indian Ocean: 1. Spatiotemporal variability of inorganic carbon and air–sea CO_2 gas exchange; *Glob. Biogeochem. Cycles* **20** GB3020.

Bey I and Jacob D J *et al.* 2001 Global modeling of tropospheric chemistry with assimilated meteorology: Model description and evaluation; *J. Geophys. Res.* **106** 23,073–23,096.

Bhattacharya S K, Borole D V, Francy R J, Allison C E, Steele L P, Krummel P, Langenfelds R, Masarie K A, Tiwari Y K and Patra P K 2009 Trace gases and CO_2 isotope records from Cabo De Rama, India; *Curr. Sci.* **97(9)** 1336–1344, http://www.jstor.org/stable/24109728.

Bhuvanachandra A, Krishnapriya M, Nayak R K and Dadhwal V K 2016 Spatio-temporal variability of atmospheric CO_2 over India and its surroundings based on satellite measurements and numerical modeling; *Proc. SPIE-9876, Remote Sensing of the Atmosphere, Clouds and Precipitation* VI:98761K, https://doi.org/10.1117/12.2223842.

Biswas H, Mukhopadhyay S K, De T K, Sen S and Jana T K 2004 Biogenic control on the air–water carbon dioxide exchange in the Sundarban mangrove environment, northeast coast of Bay of Bengal, India; *Limnol. Oceanogr.* **49** 95–101.

Cao L *et al.* 2017 The temporal and spatial distributions of the near-surface CO_2 concentrations in central Asia and analysis of their controlling factors; *Atmosphere* **8** 85, https://doi.org/10.3390/atmos8050085.

Cervarich M, Shu S, Jain A K, Arneth A, Canadell J, Friedlingstein P, Houghton R A, Kato E, Koven C, Patra P, Poulter B, Sitch S, Stocker B, Viovy N, Wilt-shire A and Zeng N 2016 The terrestrial carbon budget of south and southeast Asia; *Environ. Res. Lett.* **11** 105006, https://doi.org/10.1088/1748-9326/11/10/105006.

Deng F, Jones D B A, Henze D K, Bousserez N, Bowman K W, Fisher J B, Nassar R, O'Dell C, Wunch D, Wennberg P O, Kort E A, Wofsy S C, Blumenstock T, Deutscher N M, Griffith D W T, Hase F, Heikkinen P, Sherlock V, Strong K, Sussmann R and Warneke T 2014 Inferring regional sources and sinks of atmospheric CO_2 from GOSAT XCO_2 data; *Atmos. Chem. Phys.* **14** 3703–3727, https://doi.org/10.5194/acp-14-3703-2014.

Dettinger M D and Ghil M 1998 Seasonal and interannual variations of atmospheric CO_2 and climate; *Tellus Ser. B* **50** 1–24.

Diallo M, Legras B, Ray E, Engel A and Añel J A 2017 Global distribution of CO_2 in the upper troposphere and stratosphere; *Atmos. Chem. Phys.* **17** 3861–3878, https://doi.org/10.5194/acp-17-3861-2017.

Fan S, Gloor M, Mahlman J, Pacala S, Sarmiento J, Takahashi T and Tans P 1998 A high terrestrial carbon sink in North America implied by atmospheric and oceanic carbon dioxide data and models; *Science* **282** 442–446.

Feely R A *et al.* 1987 Distribution of chemical tracers in the eastern equatorial Pacific during and after the 1982/1983 ENSO event; *J. Geophys. Res.* **92** 6545–6558, https://doi.org/10.1029/JC092iC06p06545.

Francey R J, Tans P P, Allison C E, Enting I G, White J W C and Troller M 1995 Changes in oceanic and terrestrial carbon uptake since 1982; *Nature* **373** 326–330.

Gadgil S and Gadgil S 2006 The Indian monsoon, GDP and agriculture; *Econ. Polit. Wkly.* 4887–4895.

Ghosh S, Vittal H, Sharma T, Karmakar S, Kasiviswanathan K S and Dhanesh Y *et al.* 2016 Indian summer monsoon rainfall: implications of contrasting trends in the spatial variability of means and extremes; *PLoS ONE* **11**(**7**) e0158670.

Gloor M, Fan S M, Pacala S, Sarmiento J and Ramonet M 1999 A model-based evaluation of inversions of atmospheric transport, using annual mean mixing ratios, as a tool to monitor fluxes of nonreactive trace substances like CO_2 on a continental scale; *J. Geophys. Res.* **104** 14,245–14,260.

Houghton R A and Goodale C L 2004 Effects of land-use change on the carbon balance of terrestrial ecosystems; *Geophys. Monogr.* **153** 85–98, https://doi.org/10.1029/153GM08.

Hungershoefer K, Breon F M, Peylin P, Chevallier F, Rayner P, Klonecki A, Houweling S and Marshall J 2010 Evaluation of various observing systems for the global monitoring of CO_2 surface fluxes; *Atmos. Chem. Phys.* **10** 10,503–10,520, https://doi.org/10.5194/acp-10-10503-2010.

Idso C D, Idso S B, Kimball B A, Park H S, Hoober J K, Balling Jr RC 2000 Ultra-enhanced spring branch growth in CO_2-enriched trees: Can it alter the phase of the atmosphere's seasonal CO_2 cycle? *Environ. Exp. Botany* **43** 91–100.

Imasu R and Tanabe Y 2018 Diurnal and seasonal variations of carbon dioxide (CO_2) concentration in urban, suburban, and rural areas around Tokyo; *Atmosphere* **9**(**10**) 367, https://doi.org/10.3390/atmos9100367.

Jain S K, Agarwal P K and Singh V P 2007 Physical environment of India; In: *Hydrology and water resources of India; Water Science and Technology Library* **57**, Springer, Dordrecht.

Jiang X, Chahine M T, Olsen E T, Chen L and Yung Y L 2010 Interannual variability of mid-tropospheric CO_2 from atmospheric infrared sounder; *Geophys. Res. Lett.* **37** L13801, https://doi.org/10.1029/2010GL042823.

Jiang X, Wang J, Olsen E T, Liang M, Pagano T S, Chen L, Licata S J and Yung Y L 2013 Influence of El Nino on mid-tropospheric CO_2 from atmospheric infrared sounder and model; *J. Atmos. Sci.* **70** 223–230.

Jiang X, Crisp D, Olsen E T, Kulawik S S, Miller C E, Pagano T S, Liang M and Yung Y L 2016 CO_2 annual and semiannual cycles from multiple satellite retrievals and models; *Earth Space Sci.* **3**(**2**) 78–87, https://doi.org/10.1002/2014EA000045.

Jha C S, Thumaty K C, Rodda S R, Sonakia A and Dadhwal V K 2013 Analysis of carbon dioxide, water vapour and energy fluxes over an Indian teak mixed deciduous forest for winter and summer months using eddy covariance technique; *J. Earth Syst. Sci.* **122** 1259–1268.

Jones C D *et al.* 2003a Uncertainty in climate–carbon-cycle projections associated with the sensitivity of soil respiration

to temperature; *Tellus Ser. B* **55** 642–648, https://doi.org/10.1034/j.1600-0889.2003.01440.x.

Jones C D, Cox P M, Essery R L H, Roberts D L and Woodage M J 2003b Strong carbon cycle feedbacks in a climate model with interactive CO_2 and sulphate aerosols; *Geophys. Res. Lett.* **30** 1479, https://doi.org/10.1029/2003GL016867.

Keeling C D, Whorf T P, Wahlen M and van der Plicht M 1995 Interannual extremes in the rate of rise of atmospheric carbon dioxide since 1980; *Nature* **375** 666–670.

Keeling C D, Piper S C, Bacastow R B, Wahlen M, Whorf T P, Heimann M and Meijer H A 2005 Atmospheric CO_2 and $^{13}CO_2$ exchange with the terrestrial biosphere and oceans from 1978 to 2000: Observations and carbon cycle implications; In: *A history of atmospheric CO_2 and its effects on plants, animals, and ecosystems* (eds) Baldwin I T, Caldwell M M, Heldmaier G, Jackson R, Lange O L, Mooney H A, Schulze E D, Sommer U, Ehleringer J, Denise Dearing M and Cerling T, Springer, New York, pp. 83–113.

Keenan T F, Prentice I C, Canadell J G, Williams C A, Wang H, Raupach M and Collatz G J 2016 Recent pause in the growth rate of atmospheric CO_2 due to enhanced terrestrial carbon uptake; *Nat. Commun.* **7** 13428, https://doi.org/10.1038/ncomms13428.

Kong S, Lu B and Han B *et al.* 2010 Seasonal variation analysis of atmospheric CH_4, N_2O and CO_2 in Tianjin offshore area*; Sci. China Earth Sci.* **53** 1205.

Krishnapriya M, Bhuvanachandra A, Nayak R K, Patel N R, Rao P V N and Dadhwal V K 2017 Seasonal and interannual variability of atmospheric CO_2 based on NOAA Carbon Tracker analysis and satellite observations; *J. Indian Soc. Remote Sens.* **46(2)** 309–320, https://doi.org/10.1007/s12524-017-0688-4.

Kuze A, Suto H, Nakajima M and Hamazaki T 2009 Thermal and near infrared sensor for carbon observation Fourier-transform spectrometer on the greenhouse gases observing satellite for greenhouse gases monitoring; *Appl. Opt.* **48** 6716–6733.

LeQuéré C *et al.* 2018 Global carbon budget 2017; *Earth Syst. Sci. Data* **10** 405–448.

Lin S J and Rood R B 1996 Multidimensional flux-form semi-Lagrangian transport schemes; *Mon. Wea. Rev.* **124** 2046–2070.

Li K F, Tian B, Waliser D E and Yung Y L 2010 Tropical mid-tropospheric CO_2 variability driven by the Madden–Julian oscillation; *Proc. Nat. Acad. Sci.* **107(45)** 19,171–19,175, https://doi.org/10.1073/pnas.1008222107/-/DCSupplemental.

Li Z, Xia J, Ahlström A, Rinke A, Koven C, Hayes D J and Ji D *et al.* 2018 Non-uniform seasonal warming regulates vegetation greening and atmospheric CO_2 amplification over northern lands; *Environ. Res. Lett.* **13(12)** 124008, https://doi.org/10.1088/1748-9326/aae9ad.

Miyazaki K, Patra P K, Takigawa M, Iwasaki T and Nakazawa T 2008 Global-scale transport of carbon dioxide in the troposphere; *J. Geophys. Res.* **113** D15301, https://doi.org/10.1029/2007JD0095-57.

Mukhopadhyay S K, Biswas H, De T K, Sen B K, Sen S and Jana T K 2002 Impact of Sundarban Mangrove biosphere on the carbon dioxide and methane mixing ratio at the NE coast of Bay of Bengal, India; *Atmos. Environ.* **36** 629–638.

Nassar R, Jones D B A, Suntharalingam P, Chen J M, Andres R J, Wecht K J, Yantosca R M, Kulawik S S, Bowman K W, Worden J R, Machida T and Matsueda H 2010 Modeling global atmospheric CO_2 with improved emission inventories and CO_2 production from the oxidation of other carbon species; *Geosci. Model Dev. Discuss.* **3** 889-948, https://doi.org/10.5194/gmdd-3-889-2010.

Nayak R K, Patel N R and Dadhwal V K 2015 Spatio-temporal variability of net ecosystem productivity over India and its relationship to climatic variables; *Environ. Earth Sci.* **74(2)** 1743–1753, https://doi.org/10.1007/s12665-015-4182-4.

Nayak R K, Mishra N and Dadhwal V K *et al.* 2016 Assessing the consistency between AVHRR and MODIS NDVI datasets for estimating terrestrial net primary productivity over India; *J. Earth Syst. Sci.* **125(6)** 1189–1204, https://doi.org/10.1007/s12040-016-0723-9.

Oda T, Maksyutov S and Andres R J 2018 The open-source data inventory for anthropogenic CO_2, version 2016 (ODIAC2016): A global monthly fossil fuel CO_2 gridded emissions data product for tracer transport simulations and surface flux inversions; *Earth Syst. Sci. Data* **10** 87–107, https://doi.org/10.5194/essd-10-87-2018.

Parthasarthy B 1984 Inter-annual and long-term variability of Indian summer monsoon rainfall; *Proc. Indian Acad. Sci. (Earth Planet. Sci.)* **93** 371–385.

Potter C S *et al.* 1993 Terrestrial ecosystem production: A process model based on global satellite and surface data; *Global Biogeochem. Cycle* **7** 811–841.

Raupach M R, Marland G, Ciais P, Le Quere C, Canadell J G, Klepper G and Field C B 2007 Global and regional drivers of accelerating CO_2 emissions; *Proc. Natl. Acad. Sci.* **104(24)** 10,288–10,293, https://doi.org/10.1073/pnas.0700609104.

Rayner P and Law R 1999 The interannual variability of the global carbon cycle; *Tellus B* **51** 210–212.

Rodda S R, Thumaty K C, Jha C S and Dadhwal V K *et al.* 2016 Seasonal variations of carbon dioxide, water vapor and energy fluxes in tropical Indian Mangroves; *Forests* **7** 35.

Sabine C L, Feely R A, Gruber N, Key R M, Lee K H, Bullister J L, Wanninkhof R, Wong C S, Wallace D W R, Tilbrook B, Millero F J, Peng T H, Kozyr A, Ono T and Rios A F 2004 The oceanic sink for anthropogenic CO_2; *Science* **305** 367–371.

Sarma V V S S, Lenton A, Law R M, Metzl N, Patra P K, Doney S, Lima I D, Dlugokencky E, Ramonet M and Valsala V 2013 Sea–air fluxes in the Indian Ocean between 1990 and 2009; *Biogeoscience* **10** 7035–7052.

Schott F A and McCreary J P 2001 The monsoon circulation of the Indian Ocean, *Prog. Oceanogr.* **51** 1–123.

Smil V 2002 *The Earth's biosphere: Evolution, dynamics, and change*; MIT Press, Cambridge, 107p, ISBN 978-0-262-69298-4.

Suntharalingam P, Jacob D J, Palmer P I, Logan J A, Yantosca R M, Xiao Y, Evans M J and Streets D G *et al.* 2004 Improved quantification of Chinese carbon fluxes using CO_2/CO correlations in Asian outflow; *J. Geophys. Res.* **109** D18S18, https://doi.org/10.1029/2003JD004362.

Takagi H *et al.* 2014 Influence of differences in current GOSAT XCO_2 retrievals on surface flux estimation; *Geophys. Res. Lett.* **41** 2598–2605, https://doi.org/10.1002/2013GL059174.

Takahashi T *et al.* 2009 Climatological mean and decadal change in surface ocean pCO_2 and net sea-air CO_2 flux over

the global oceans; *Deep-Sea Res. Pt. II,* https://doi.org/10.1016/j.dsr2.2008.12.009.

Tans P P *et al.* 1990 Observational constraints on the global atmospheric CO_2 budget, *Science* **247** 1431–1438.

Tiwari Y K, Patra P K, Chevallier F, Francey R J, Krummel P B and Allison C E *et al.* 2011 CO_2 observations at Cape Rama, India for the period of 1993–2002: Implications for constraining Indian emissions; *Curr. Sci.* **101** 1562–1568.

Tiwari Y K, Vellore R K, Ravi Kumar K, van der Schoot M and Cho C H 2014 Influence of monsoons on atmospheric CO_2 spatial variability and ground-based monitoring over India; *Sci. Total Environ.* **490** 570–578, https://doi.org/10.1016/j.scitotenv.2014.05.045.

Van der Werf G R, Randerson J T, Giglio L, Collatz G J, Kasibhatla P S and Arellano Jr A F 2006 Inter-annual variability in global biomass burning emissions from 1997 to 2004; *Atmos. Chem. Phys.* **6** 3423–3441.

Valsala V and Maksyutov S 2013 Inter-annual variability of the air–sea CO_2 flux in the north Indian Ocean; *Ocean Dyn.* **63** 165–178.

Watanabe H, Hayashi K, Saeki T, Maksyutov S, Nasuno I, Shimono Y, Hirose Y, Takaichi K, Kanekon S, Ajiro M, Matsumoto Y and Yokota T 2015 Global mapping of greenhouse gases retrieved from GOSAT Level 2 products by using a kriging method; *Int. J. Remote Sens.* **36(6)** 1509–1528, https://doi.org/10.1080/01431161.2015.1011792.

Yevich R and Logan J A 2003 An assessment of biofuel use and burning of agricultural waste in the developing world; *Global Biogeochem. Cycle* **17(4)** 1095.

Yokota T, Yoshida Y, Eguchi N, Ota Y, Tanaka T, Watanabe H and Maksyutov S 2009 Global concentrations of CO_2 and CH_4 retrieved from GOSAT: First preliminary results; *Sci. Online Lett. Atm.* **5** 160–163.

Yoshida Y, Ota Y, Eguchi N, Kikuchi N, Nobuta K, Tran H, Morino I and Yokota T 2011 Retrieval algorithm for CO_2 and CH_4 column abundances from short-wavelength infrared spectral observations by the Greenhouse gases observing satellite; *Atmos. Meas. Tech.* **4** 717–734, https://doi.org/10.5194/amt-4-717-2011.

Yoshida Y, Kikuchi N, Morino I, Uchino O, Oshchepkov S, Bril A, Saeki T, Schutgens N, Toon G C, Wunch D, Roehl C M, Wennberg P O, Griffith D W T, Deutscher N M, Warneke T, Notholt J, Robinson J, Sherlock V, Connor B, Rettinger M, Sussmann R, Ahonen P, Heikkinen P, Kyrö E, Mendonca J, Strong K, Hase F, Dohe S and Yokota T 2013 Improvement of the retrieval algorithm for GOSAT SWIR XCO_2 and XCH_4 and their validation using TCCON data; *Atmos. Meas. Tech.* **6** 1533–1547, https://doi.org/10.5194/amt-6-1533-2013.

Zimov S A *et al.* 1999 Contribution of disturbance to high-latitude amplification of atmospheric CO_2; *Science* **284** 1973–1976.

Corresponding editor: C Gnanaseelan